

1 **Mapping of submerged aquatic vegetation in rivers from very high resolution image data, using**
2 **Object Based Image Analysis combined with expert knowledge**

3 Fleur Visser^{1*}, Kerst Buis², Veerle Verschoren², Jonas Schoelynck²

4

5 Affiliations+ addresses of authors:

6 1) Institute of Science and the Environment, University of Worcester, Henwick Grove, Worcester
7 WR2 6AJ, UK

8 2) Department of Biology, Ecosystem Management Research Group, University of Antwerp,
9 Universiteitsplein 1C, B-2610 Wilrijk, Belgium;

10

11 Contact details corresponding author:

12 *f.visser@worc.ac.uk; Tel.: +44-1905-855236.

13

14 Abstract

15 The use of remote sensing for monitoring of submerged aquatic vegetation (SAV) in fluvial
16 environments has been limited by the spatial and spectral resolution of available image data. The
17 absorption of light in water also complicates the use of common image analysis methods. This paper
18 presents the results of a study that uses very high resolution (VHR) image data, collected with a Near
19 Infrared sensitive DSLR camera, to map the distribution of SAV species for three sites along the
20 Desselse Nete, a lowland river in Flanders, Belgium. Plant species, including *Ranunculus aquatilis* L.,
21 *Callitriche obtusangula* Le Gall, *Potamogeton natans* L., *Sparganium emersum* L. and *Potamogeton*
22 *crispus* L., were classified from the data using Object-Based Image Analysis (OBIA) and expert
23 knowledge. A classification rule set based on a combination of both spectral and structural image

24 variation (e.g. texture and shape) was developed for images from two sites. A comparison of the
25 classifications with manually delineated ground truth maps resulted for both sites in 61% overall
26 accuracy. Application of the rule set to a third validation image, resulted in 53% overall accuracy.
27 These consistent results show promise for species level mapping in such biodiverse environments, but
28 also prompt a discussion on assessment of classification accuracy.

29 Keywords

30 Macrophytes; OBIA; Remote Sensing; VHR image data; knowledge-based

31 Introduction

32 Until recently remote sensing has rarely been used as tool for monitoring of submerged aquatic
33 vegetation (SAV) in fluvial environments. This is partly due to the limited spatial resolution of image
34 data produced by conventional sensor/platform combinations. Another problem is the absorption of
35 light in water, particularly in wavelengths most suitable for vegetation detection, which complicates
36 the use of common image analysis methods (Lucas & Goodman, 2014). Several recent technological
37 developments are now enabling researchers to overcome some of these issues. Firstly the rapid
38 development in remote sensing platforms such as Unmanned Aerial Systems (UAS) now allows
39 collection of very high resolution (VHR) image data of (sub-)centimetre resolution with wavelength
40 bands beyond the visible light (e.g. Lucieer et al., 2014). In addition to this the relatively new Object
41 Based Image Analysis (OBIA) approach can be used to derive information from images, while relying
42 less on spectral information only (e.g. Laliberte et al., 2011).

43 The OBIA method works by first segmenting an image into objects that consist of groups of spectrally
44 similar and adjacent pixels, rather than classifying an image on a pixel by pixel basis. The objects
45 formed this way will vary in shape and size, depending on the underlying image and the segmentation
46 algorithm used, and therefore provide an extra spatial dimension to the data, which can benefit image
47 interpretation. The approach works particularly well in combination with VHR image data, which is
48 now more commonly available (Blaschke, 2010). A close up of a river section with two different

49 vegetation species (*Callitriche obtusangula* Le Gall and *Ranunculus aquatilis* L.) shown in Figure 1,
50 helps illustrating the advantage of OBIA compared with pixel-based image analysis. Due to the
51 variable, but comparable spectral values of the two plants it is difficult to classify individual pixels as
52 belonging to either of the two species. However, a trained observer can readily identify what part of
53 the section is covered in which species, based on additional image detail such as leaf and stem shapes.
54 OBIA can include this kind of contextual information during the object-based image analysis process
55 and therefore seems a promising contribution to the development of an automated detection tool for
56 Submerged Aquatic Vegetation (Visser et al., 2013).

57 Only recently OBIA is being applied specifically for the detection and classification of SAV.
58 However, these studies are so far mostly undertaken in coastal environments (e.g. Klemas, 2013;
59 Roelfsema et al., 2014) and few involve classification of image data beyond plant functional level
60 (e.g. Dronova et al., 2012). A review of methods used for plant species classification, also showed
61 that few studies make use of VHR images in order to derive specifically geometric attributes of
62 objects to enhance a classification (Dronova, 2015). The authors of this paper argue that classification
63 through knowledge-based rule sets, which exploit such attributes/features, is a particular strength of
64 OBIA and should be explored further. Visser et al. (2013) already showed how the approach can
65 improve SAV detection compared to classification based on spectral information only. With the study
66 presented in this paper we aim to show how a multi-level knowledge-based OBIA can provide a
67 practical approach to map complex SAV communities at species level in a clear water stream.

68 Methods

69 Study site

70 Data for this study were obtained from the Desselse Nete, which is a lowland stream in Flanders,
71 Belgium with an average water depth of approximately 0.6-0.7 m, a mean width of 6.2 m and a mean
72 discharge of 0.3 - 0.6 m³ s⁻¹. The river has generally low suspended solid and organic matter
73 concentrations (<50 mg/l). Three river sections of approximately 5 x 5 m length were selected close to

74 its confluence with the Zwarte Nete near the village of Retie. Data were collected in May 2012, when
75 the vegetation on one sample site consisted of dense submerged patches of Water Crowfoot
76 (*Ranunculus aquatilis* L.), Blunt-fruited Water Starwort (*Callitriche obtusangula* Le Gall) and Curly-
77 leaf Pondweed (*Potamogeton crispus* L.). The plants on two other sample sites were more open and
78 consisted mostly of Broad-Leaved Pondweed (*Potamogeton natans* L.), and European Bur-reed
79 (*Sparganium emersum* L.).

80 Image data acquisition

81 The specific advantages of OBIA can only be deployed in analysis of images with sufficient detail
82 (Blaschke, 2010). The method therefore works best on VHR image data. An increasingly popular type
83 of platform from which to obtain such data is an unmanned aerial system (UAS) (Anderson & Gaston,
84 2013; Woodget et al., 2015). Data collection from UAS-s is however still constrained by issues such
85 as weather conditions and the short battery life of many systems. Alternative ground-based platforms
86 such as telescopic poles, are gaining in popularity too and are not affected by such issues (e.g. Hauet
87 et al., 2009; Laliberte et al., 2007; Luscier et al., 2006; Visser et al., 2013), however their application
88 is limited by the spatial extent of images obtained from lower altitudes. For the current project spatial
89 extent was not a prerequisite, so image data was collected from a telescopic pole fixed in position
90 with guy ropes at approximately 4.5 m at nadir over the centre line of the river.

91 Earlier research has indicated the importance of near infrared (NIR) light reflectance for the detection
92 of SAV in shallow submerged environments (Visser et al., 2013). We therefore collected both colour
93 photographs (RGB) and single band NIR photographs. The photos were obtained with a Fujifilm IS-
94 Pro NIR sensitive digital single-lens reflex (DSLR) camera and a Tamron AF Aspherical 28-80 mm
95 f/3.5-5.6 lens. This camera model does not contain any internal NIR or ultraviolet (UV) blocking
96 filters and therefore senses the full spectrum of UV, visible light (VIS) and NIR light. By adding
97 different filters to the lens, selected parts of the electromagnetic spectrum can be captured by the
98 camera sensor. Red, Green and Blue image bands were obtained by adding a NIR blocking filter
99 (model XNite CC1, LDP LLC, Carlstadt, USA, formerly 'maxmax.com', here referred to as 'CC1'),
100 which transmits only visible (VIS) light, while using all three RGB sensor channels. A single band

101 covering most of the NIR spectrum (NIR(R72)) was obtained by adding a Hoya R72 VIS blocking
102 filter to the lens. A further two bandpass filters (XNite Bandpass IR Filters, LDP LLC, Carlstadt,
103 USA), were used to obtain one narrow NIR wavelength band around 710 nm (model XNite BPB, here
104 referred to as ‘NIR (BP1)’ and one around 828 nm (model XNite BPG, here referred to as
105 ‘NIR(BP2’)). Figure 2 shows the filter transmission spectra.

106 The Fujifilm IS-Pro was used in combination with a radio controlled shutter and produced photos of
107 3024x2016 pixels in 8-bit GEOTIFF format. Although RAW is seen as the preferred image format for
108 image analysis (Verhoeven, 2010) TIFF was chosen in this study because of its ease of use (format
109 and file size). Relative ambient light conditions were estimated with an ATP DT-1309 Auto Ranging
110 Light Meter.

111 Image pre-processing

112 *Radiometric data issues*

113 Due to the low altitude of the sensor platform atmospheric correction of the image data was not
114 needed. However, several other types of radiometric issues clearly affected the acquired image data,
115 which were sunglint, skyglint and specular reflection at the water surface, as well as shadows from
116 surrounding vegetation and hotspotting effects caused by the camera. Several methods exist in the
117 literature for removal of sunglint, however they were mostly developed for marine environments and
118 therefore not really suitable for small scale, shallow river environments (Kay et al., 2009; Visser et al.,
119 2015). In this study objects affected by sunglint were assigned to a separate class during rule set
120 development and that way excluded from further analysis. The authors of this paper are not aware of
121 effective methods that can be used to remove skyglint, specular reflection at the water surface, nor for
122 the removal of significant shadow effects. No attempts were therefore made to remove/reduce their
123 effect.

124 Concentric bands of lighter shades that occur in some of the NIR(BP2) images were thought to be so
125 called ‘hotspotting’ or ‘lens flaring’. This radiometric anomaly occurs due to internal reflection of
126 light between the camera, lens and possible filters and is quite commonly observed in NIR

127 photography (Verhoeven, 2008). Its occurrence is camera, lens, filter, light and aperture dependent
128 and therefore not easy to predict and avoid. Visser et al. (2015) attempted to remove the effect with
129 and image based correction method. For their study the improvement was visible but had insignificant
130 effect on the overall results.

131 In summary, as known correction approaches did not seem to significantly improve image quality, no
132 radiometric pre-processing steps were undertaken before image analysis. The effect this may have had
133 on the classification results are considered in the Discussion section.

134 *Geometric Correction*

135 Geometric correction of digital photographs usually involves a lens barrel correction, however, no
136 lens profile data was found for the Tamron lens used in this project. An alternative distortion
137 assessment on geometry in sample photographs, using Adobe Photoshop did not indicate significant
138 distortion in horizontal or vertical direction, confirming claims of Tamron (tamron-usa.com) that this
139 type of 'AF Aspherical' lens, eliminates aberrations and distortion. No correction was therefore
140 applied to the photos before undertaking further analysis.

141 To align all photos co-registration was undertaken using four fixed ground control points that were
142 included in all photos, as well as additional features that could be identified in multiple photos.

143 Second order polynomial transformations were applied to match the photographs, which resulted in
144 root mean square errors (RMSE) of 0.1 to 10 cells (\approx 0.2 to 24 mm). Some of the larger errors would
145 have been caused by lack of matching tie points within the scene in addition to the four ground
146 control points. Finding identical features in the moving water and on the grassy banks proved
147 extremely difficult. The transformed data was resampled using the Nearest Neighbour algorithm, to
148 produce final image layers. Three single band NIR and one RGB colour images were combined into a
149 multi-band image file and cropped to remove parts of the scene not covered by all four images.

150 **Object Based Image Analysis**

151 The most commonly used image classification algorithms work on a pixel-by-pixel basis, where the
152 spectral values of a pixel are used to assign that pixel to the most suitable class. By first grouping

153 adjacent pixels with similar spectral values into objects (the segmentation process) and including
154 features of those objects in the image classification process, classifications can be significantly
155 improved (Blaschke et al., 2011). Object features can be spectral values, representing average object
156 reflectance as well as within-object reflectance variability, but also geometric features such as shape
157 (e.g. roundness or length/width ratio), or internal texture and relationships to adjacent objects (e.g.
158 contrast to neighbouring object). Classifying an image using rule sets based on such feature values,
159 may better replicate the perception of an expert in the field (e.g. Blaschke, 2010; d'Oleire-Oltmanns et
160 al., 2014). These and other different theoretical foundations of OBIA compared to the 'per-pixel'
161 approach are believed to be a new paradigm in remote sensing and GIS science (Blaschke et al.,
162 2014).

163 For this study we selected two of the three sites to develop a classification rule set. Selection was
164 based on the range of vegetation types present at each site, as the validation site should not contain
165 any species that were not present at the sites used for rule set development. The sites used for rule set
166 development are referred to as site 1 and 2. The final rule set was then applied to the image of the
167 third site, site 3, to test its transferability. All three classified images were compared with manually
168 obtained reference images to assess the performance of the rule set. Further details on each of these
169 OBIA analysis steps are given in the following sections.

170 *Image segmentation*

171 In this project we used multiresolution segmentation as available in eCognition Developer software
172 (Trimble Geospatial), with which objects can take on any form during the segmentation process. The
173 shape and size of the objects are to some extent constrained by three parameters that can be set before
174 running the segmentation. These are scale, shape and compactness. A segmentation can be based on
175 the spectral values in all image data layers combined. In our analysis we applied segmentation to one
176 image data layer only, rather than a combination of the six available layers. The NIR(BP1) layer was
177 selected for this purpose, as it was noted by the experts involved that this layer allowed best
178 identification of SAV species, and therefore thought to result in most relevant object delineation. The
179 decision to use a single band for segmentation was determined by the limitations of our equipment,

180 which did not allow for simultaneous collection of all image bands. In combination with the dynamic
181 nature of the submerged vegetation this meant that plant elements such as leaves were not located in
182 exactly the same position in each image data layer and thus would not show up as distinct objects
183 during a segmentation based on multiple layers.

184 Segmentation was performed at two different levels. Each level had a clear target object size. At
185 Level 1 we aimed to delineate objects of the size of individual patches of plant species. At Level 2 we
186 aimed to delineate smaller objects representing plant morphological elements such as individual
187 leaves and stem segments. The most suitable scale parameter for each level was determined by trial
188 and error. Quite recently tools have been developed to automatically identify meaningful parameter
189 values (e.g. Drăguț et al., 2010), but mostly for scenes where there is no a priori knowledge of
190 meaningful object scales. In this study we were able to identify meaningful objects based on expert
191 knowledge of plant morphology prior to the OBIA analysis. Suitable scale parameter values were
192 therefore obtained by running segmentations with different parameter settings and choosing those that
193 provided the best results according to the expert's judgement. The chosen parameter values and
194 settings for each of the two segmentation levels are as follows:

195 Level 1: Multiresolution segmentation: Scale parameter 100; Shape 0.2 Compactness 0.2: NIR(BP1)
196 data layer only.

197 Level 2: Multiresolution segmentation: Scale parameter 20; Shape 0.2 Compactness 0.2: NIR(BP1)
198 data layer only.

199 The same values were applied to the images of each of the three sites.

200 *Classification rule set development theory*

201 After the image is segmented into image objects, the next step is to classify these objects in to the
202 correct class of a predefined class hierarchy. In our project the class hierarchy consisted of the species
203 as observed in the river sections, plus a bottom, an emergent vegetation, and some mixed vegetation
204 classes. There are many different ways in which a rule set for the object classification can be

205 developed. Some authors have used supervised classification approaches similar to those used in
206 pixel-based image analysis, where samples of objects are used to produce statistical class descriptions
207 according to which the remainder of the objects can be classified (e.g. Mui et al., 2015; Roelfsema et
208 al., 2014). However, one of the great advantages of OBIA is its suitability for knowledge based/driven
209 rule set development. In this study we particularly wanted to replicate some of the cognitive steps
210 undertaken by SAV experts in order to identify vegetation species from aerial photographs.
211 Significant advances have been made organizing and expressing domain knowledge into a machine-
212 readable format (Belgiu et al., 2014), but this approach is very much ‘work in progress’, so in this
213 study we have limited ourselves to expert rule set development using a trial and error approach (e.g.
214 Rampi et al., 2014) to test what kind of accuracy can be achieved this way. An important
215 disadvantage of this approach is the level of subjectivity and the relatively time consuming practice of
216 manually developing the rule set. A satisfactory result that proves to be transferrable and can be used
217 to map SAV over a much wider area would however strongly compensate for these shortcomings.

218 When deciding on rules and thresholds we aimed to select mostly features that would be least affected
219 by changes in image resolution and illumination conditions. Spectral object feature values used in the
220 classification were derived from individual image data layers as well as from combinations of layers.
221 It appeared however impossible to create an effective rule set without the use of thresholds involving
222 absolute spectral values from some (combination) of the six image data layers (i.e. red, green, blue,
223 NIR(BP1), NIR(BP2) and NIR(R72)), so they were included where needed. The effect this has on
224 transferability of the final rule set will be addressed in the Discussion section. Image scale will also
225 affect the effectiveness of class rule thresholds, as the size and shape of an object determines the
226 number and location of pixels included and consequently the overall object values (Li & Shao, 2014).
227 Since photos for all three sites were taken from very similar elevations, we expect the same optimal
228 scale parameter values to apply. For all types of features we have optimized class rule thresholds
229 manually through an iterative process of modifying thresholds and observing the classification results
230 for the two ‘training’ images simultaneously.

231 *Rule set development steps*

232 The flow diagram of Figure 3 shows how all objects were classified according to a predefined class
233 hierarchy, by means of a set of rules. The rules applied for each class are listed in Table 1. In the table
234 classes as used in the final SAV species maps are indicated with an 'f'. A number of intermediate
235 (temporary) classes, usually consisting of a combination of species, were also created during the
236 process. They are listed in the table with a 't'. For some classes all objects were assessed while for
237 other classes only objects previously assigned to another (temporary) class are considered. The
238 structure of this process is indicated with flow lines in Figure 3. Classes created at different
239 segmentation levels are separated in the diagram and flow lines indicate where Level 2 classes (L2)
240 are used as input for Level 1 classification (L1). A detailed motivation for the choice of features used
241 for the classification rules for each class is given below. Where multiple levels are used to identify a
242 target surface/species, this is mentioned in the motivation:

243 Bank vegetation and emergent macrophytes (f, L1) – NIR reflectance of SAV is more strongly
244 absorbed than VIS reflectance due to the overlying water column. This effect is absent from emergent
245 and terrestrial vegetation. NDVI is a feature commonly used in remote sensing to differentiate
246 vegetated from non-vegetated surfaces. In a similar way this feature allows for separation between
247 emergent and submerged vegetation. As its value is made up of a ratio of image bands it can be
248 considered a relative spectral measure. NDVI values are negative for all aquatic classes while
249 emergent and terrestrial vegetation have positive values. NIR(R72) has the strongest reflectance for
250 emergent and terrestrial vegetation, which makes the mean of this band useful for separation from
251 submerged aquatic vegetation.

252 Bottom (f, L1) – Parts of the images representing the river bed generally have very low reflectance
253 values, particularly in the longer wave NIR band (i.e. NIR(BP2)), therefore a threshold value for this
254 band was selected. This type of surface also tends to be very homogeneous, compared to other
255 surfaces, particularly in the NIR(R72) band. The standard deviation for this band is therefore selected
256 as a second selection criterion for bottom objects.

257 *C. obtusangula/R. aquatilis/P. crispus* (t, L1) – These three species all seem to reflect particularly
258 strongly in the NIR(BP1) band, so this band is used to isolate objects that definitely aren't either of
259 these species (i.e. low NIR(BP1)).

260 *P. crispus* (f, L1) – This plant has a curly leaf, which is most distinct in the NIR(BP1) band where the
261 undulating leaf surface creates clear spectral contrast, which can be quantified by means of the
262 standard deviation of this feature.

263 *P. natans* (f, L1+L2) – The most distinct characteristic of the *P. natans* plant are its floating oval
264 shaped leaves. At the Level 2 segmentation these leaves are delineated and can be classified through a
265 combination of rules relating to the object roundness; area (<450 pxl); $90 < \text{Brightness} < 134$; Their
266 relatively short length (< 50 pxl); a specific length/width ratio and a distinct difference in colour to
267 neighbouring object, particularly in band NIR(BP1) < 4. Brightness is calculated as the 'mean value
268 of the spectral mean values of an image object' (Definiens AG, 2007).

269 *S. emersum* (f, L1+L2) – The leaves of this plant are very narrow and highly reflectant, which enables
270 delineation and classification at the level of individual leaves. Features used are length/width ratio,
271 absolute width, relative border to brighter objects in NIR(BP1). The latter feature represents the
272 length of the shared border of neighbouring image objects with a higher brightness value. Also the
273 absolute mean value of NIR(BP1) is used, as this is the layer in which the objects show up clearest.

274 *S. emersum* and *P. natans* mix (f, L1) – Due to the nature of these two species they locally form a
275 very homogeneous mixture, which makes it nearly impossible to separately map each species. For
276 these situations a separate mixed class has been allocated, which is dependent on the presence of a
277 minimum number/area cover of sub objects for each of the two species.

278 *C. obtusangula / R. aquatilis* (t, L1) – Objects that potentially are *C. obtusangula* or *R. aquatilis* are
279 assigned to this temporary class based on the shape of their sub objects and reflectance in the red
280 band.

281 *C. obtusangula* (f, L1+L2) – This plant has distinct rosette shaped leaves, which are delineated as
282 round/square objects at Level 2 with a particularly low length/width ratio (<2). The actual plant
283 objects at Level 1 can be identified by the relative area taken up by the rosettes, in combination with
284 the absence of Level 2 *P. natans* leaf sub-objects. Only objects previously classified as *C.*
285 *obtusangula* / *R. aquatilis* / *P. crispus* are used as input.

286 *R. aquatilis* (f, L1+L2) – This species can be recognised in photos by its highly reflectant stem
287 surrounded by furry leaves. The number of elongated leaves/stems is used to separate *R. aquatilis*
288 objects from the *C. obtusangula* / *R. aquatilis* / *P. crispus* class.

289 Sunlint (f, L1) – Sunlint shows in the image as white light, which means high values in all three
290 visible image bands. The intensity of these three bands combined is represented by the Brightness
291 value. A high threshold of 160 effectively classifies all sunlint objects. Some exposed surfaces with
292 similar brightness values, were previously classified as exposed and therefore excluded from this step.

293 Exposed bank/Oat flakes on bed (f, L1) – Soil, as visible at exposed banks, has a distinct high red
294 reflectance, which is a common characteristic. This class also included patches of oat flakes deposited
295 on the river bed after flow velocity assessments using oat flake particles, which took place during the
296 same field data collection campaign. The spectral characteristics of the oat flakes were similar to
297 those of exposed soil.

298 Vegetation general (f, L1) – Of the temporary class *C. obtusangula/R. aquatilis/P. crispus* (t, L1)
299 objects that were not redistributed to other classes were classified as ‘Vegetation general’ as they were
300 thought to be some form of vegetation that could not be identified in more detail through rules. This
301 class was not used in the manually obtained reference maps, as experts were able to identify dominant
302 species cover for all polygons.

303 Bar (f, L1) – The metal bar across the river which is visible in the image of site 2, could be classified
304 effectively based on the extremely elongated shape of the polygons it is made up of.

305 Comparison of classification results with manually derived SAV maps

306 The reliability of the knowledge-based OBIA approach was assessed by comparing the classification
307 results for each of the three sites with maps, in which vegetation classes have been manually
308 delineated. For remote sensing classification studies accuracy assessments are usually done by taking
309 a sample of pixels from across the classes represented in the image. Based on this sample an error
310 matrix is calculated, from which then an overall accuracy and kappa coefficient are calculated. The
311 former is the percentage of correctly classified pixels and the latter coefficient supposedly provides a
312 similar measure, but adjusted for agreement occurring by chance. Although still commonly applied,
313 the usefulness of the kappa coefficient has recently come under debate (Olofsson et al., 2014) and is
314 there for not used in this paper. For OBIA classifications it is generally accepted that the sampling
315 units should consist of polygons rather than pixels (Radoux et al., 2011), however a universally
316 accepted method to compare classification and reference polygons when they can differ both in size
317 and class definition, has not yet been devised. A slightly exceptional situation in this study occurred
318 due to the fact that the manually obtained reference data covers the full classification area, which
319 means a direct comparison between the two data layers can be made and no inferential statistics is
320 needed to estimate the accuracy of the classification. When doing a comparison based on polygon
321 units however, a problem could still arise, as the automatic classification polygons would not
322 necessarily line-up with the manually delineated polygons, which would result in positional as well as
323 thematic differences and are difficult to tackle simultaneously. Instead we decided to create a manual
324 reference layer by using the Level 1 segmentation polygons and manually classify each polygon,
325 referring to each of the six image data layers for confirmation, as well as to overview sketches of the
326 patch distribution and species composition, which were made in the field.

327 During the classification process it was observed that some polygons were under-segmented as these
328 polygons clearly consisted of more than one class, which dominated in distinctly different parts of the
329 polygon. For such polygons an expert would have decided to separate the classes with an additional
330 boundary, but this was not possible due to the segmentation framework. In these situations the
331 polygon was given the class value of the most dominant species appearing in that polygon. Where
332 species cover was too low or too difficult to distinguish, the polygons were classed as Bottom.

333 To evaluate the transferability of our approach we were particularly interested to see how similar the
334 validation classification of site 3 is to the manual map of site 3 compared to the comparisons for the
335 two sites, used for rule set creation.

336 Results

337 Figure 4 shows close-ups of the Level 2 segmentation and classification, as used in the image analysis
338 procedure. Figures 5-7 show the final classification results for each of the three sites, together with the
339 manually delineated class maps, as well as the NIR(BP1) image source data layer. The classification
340 results clearly bring out the different composition of the vegetation communities found at each of the
341 sites as, well as the more mixed cover type found on site 3.

342 The overall accuracy coefficient shows the agreement between the OBIA-derived classification map
343 and manual reference data (Table 2). The coefficient is highest for the classification of site 1 and
344 lowest for that of site 3. All values are below what is generally seen as an acceptable level of accuracy
345 for an image classification even compared to other studies undertaken under the challenging
346 conditions provided by submerged aquatic environments (Dronova, 2015; Husson et al., 2014).

347 Looking at the classification accuracies for individual species (Table 3) they vary between sites.

348 User's and producer's accuracies (UA and PA) are the best measures to evaluate these. For example
349 the classification of bottom for site 1 has a very high UA (0.98), meaning that there is a high
350 likelihood that an automatic classification result corresponds with the reference map. Looking
351 however at the PA this is considerably lower (0.69), because many of the bottom polygons on the
352 reference map have not been correctly classified by the automatic classification. When assessing all
353 other classes in a similar way some classes perform better than others. The class 'Bank vegetation and
354 exposed macrophytes' seems to be classified best as for all three sites both the UA and PA are
355 amongst the top three highest, with values ranging between 0.70 and 0.93. Bottom also seems well
356 classified, for site 1 and 2 (0.69 to 0.98), but both UA and PA are low for site 3 (0.57 and 0.29). For
357 the latter site bank and bottom are often misclassified as vegetation general and several polygons were
358 classified by the expert as sunglint, but by the algorithm as bottom. Consequently sunglint has a very

359 low PA for this site (0.28). At site 2 this class performs better, with almost 100% accuracy, while at
360 site 1 sunglint is classified by the algorithm but not observed by the expert. The best performing
361 vegetation species is *P. crispus*, but this species was only observed at site 1 (UA = 0.50 and PA =
362 0.64). *C. obtusangula* only occurs on site 1 (UA = 0.5 and PA = 0.76) and 3 (UA = 0.44 and PA =
363 0.47). For both sites most confusion occurs with *R. aquatilis*. In the mixed class most confusion
364 occurs with the pure *P. natans* and *S. emersum* as could be expected since that is what the mix
365 consists of. The pure *P. natans* and *S. emersum* classes have reasonable UAs and PAs ranging
366 between (0.41 and 0.68) for site 2 and 3, but lower ones for site 2 where the values are highly variable
367 (between 0.00 and 0.5). This is most likely due to the absence of the species there resulting in a low
368 number of misclassifications which leads to low UA and PA values. At site 1 where *R. aquatilis* was
369 most dominant the UA for this species was high (0.82), however many patches identified by the
370 expert were misclassified as bank, vegetation general or *S. emersum* resulting in a PA of only 0.29.
371 The species did not perform any better on the other sites (UA and PA between 0.67 and 0.11). The
372 class vegetation general picked up polygons that did not fit in any of the other (vegetation) classes.
373 Across all sites in particular polygons classified as bottom by the expert ended up in this class, but
374 also *R. aquatilis*, *P. natans* and the mixed class were misclassified. .

375 Discussion

376 Classification accuracy

377 The results of this study show that OBIA has potential to aid mapping of SAV in clear-water streams.
378 The most promising result is a rather consistent overall accuracy of 53-61% for both the sites used in
379 the development of the classification rule set and the validation site. Although for remote sensing
380 classification studies an overall accuracy >85% is generally set as a target level, this is rarely attained
381 (Foody, 2012) and these standards have been devised for terrestrial environments that do not suffer
382 from complicating factors experienced in aquatic environments, such as absorption of light by water.
383 So despite the relatively low similarities between the OBIA classification and the manually produced

384 maps we consider the results as promising with more than half of each image correctly classified. In
385 particular because a single rule set was used to achieve this, we think it is an acceptable result that
386 warrants further investigation of the approach.

387 Considering only those vegetation classes that were observed by the expert at either site, it is difficult
388 to find one or more that consistently perform worst. There also do not seem to be any very consistent
389 confusions/misclassifications. This makes it difficult to provide useful recommendations on how the
390 rule set may be modified to improve the results. The use of multi-level classification and
391 segmentation, which identified specific plant morphological elements shows promise to tackle the
392 canopy complexity, however, further research is needed to identify the most appropriate rules that can
393 characterise/formalize boundaries within and between patches of mixed vegetation. Furthermore some
394 very deep *S. emersum* and *P. natans* was identified by the expert, but appeared not sufficiently distinct
395 to be included in the segmentation and classification as distinct objects/patches, which will have
396 influenced the accuracy results. Further gains in improvement of the classification probably require
397 improvement of the data quality as will be discussed in the following sections.

398 Image data quality

399 An important factor that needs to be considered when evaluating the classification results is the
400 quality of the image data used. In this case image data was collected with a consumer-grade digital
401 camera and a set of separate filters. The various image layers used in the analysis were therefore not
402 collected simultaneously. As a result the image elements such as individual plant leaves are not in
403 exactly the same location in four of the six bands used, due to movement of the plants with the river
404 current. This will have significantly affected the image segmentation and the effectiveness of certain
405 rules used. All segmentation was done on one layer only, while rules were developed using multiple
406 layers as well as different individual layers. For example one of the rules used to create the temporary
407 class '*C. obtusangula* / *R. aquatilis*', is based on a range of values for the mean red band. It is very
408 likely that this rule would be more effective if plant leaves and stems in the red band would be
409 positioned in exactly the same location as in the NIR(BP1) band and thus line up exactly with object
410 boundaries. Data collected with a multi-spectral optical sensor of sufficient spatial and spectral

411 resolution will therefore most likely result in a significant increase in classification accuracy. The
412 advantage of the method demonstrated here is however its cost effectiveness and relatively low
413 weight. It is possible for one person to carry the set up applied here (or to attach to an UAS) and that
414 way collect images over much larger areas.

415 A number of different factors affected the radiometric values of the image data, including sunglint
416 skyglint, specular reflection, hotspotting and shading. Sunglint was effectively identified during the
417 image classification process for site 2 (PA = 0.80 and UA 1.00), though slightly less well site 3 (PA =
418 0.28 and UA = 0.78). These results suggest that by applying a classification rule sunglint-affected
419 objects can be identified and eliminated during further application of the classification results.
420 Information of vegetation cover is however lost for these locations, so final cover maps would involve
421 interpolation of some kind. The presence of adjacency effects such as the reflection of vegetation at
422 the water surface is particularly strongly visible in the NIR and may have influenced the segmentation
423 based on the NIR(BP1) band. Until an effective way has been developed to remove/avoid such
424 effects, this will remain a significant issue for remote sensing in river environments where the
425 distance between any part of the water surface and surround terrestrial vegetation is generally small.
426 Since the flaring/hotspotting effect only occurred in band NIR(BP2) it did not show up in the
427 segmentation patterns and as this band was not often selected as feature in classification rules we
428 expect that it had little or no effect on the classification results. Pre-processing to remove this effect is
429 deemed unnecessary. Photos for this project were collected under suboptimal conditions and some are
430 therefore affected by skyglint and/or shading. These effects were not clearly visible in the delineation
431 of image segments, but may have affected the effectiveness of rules based on absolute spectral values.
432 Ideally these kinds of effects should be reduced by choosing the right time of the day and clear sky
433 conditions for image data collection. This is however not always achievable due to time constraints on
434 data collection, as was the case with this project. The occurrence of skyglint and/or shading will affect
435 most types of remote sensing, however, because of its reduced reliance on spectral information, the
436 OBIA method proposed here may actually be relatively insensitive to these kind of issues.

437 Another important factor that will affect the collection of images of sufficient quality and has
438 influenced the presented results to some extent, is its reliance on clear and shallow waters. This is a
439 universal issue affecting the application of optical remote sensing approaches in aquatic
440 environments. In our classification we experienced difficulties delineating and classifying the deeper
441 vegetation patches. Shallow water is however the environment where the method would be of most
442 benefit, as this is where the greatest diversity of SAV can be expected, so there will be a sufficiently
443 large environment for which the method can be very suitable. Finally the current resolution and 2D
444 nature of most remote sensing data does not provide enough detail to enable assessment of the large
445 amount of morphological variation that can be found amongst certain SAV species, making them
446 nearly impossible to identify. Where these boundaries for SAV classification lie requires further
447 investigation.

448 Application potential

449 The fact that one rule set was created, which consistently performed moderately well on three rather
450 different scenes suggest that this approach may be transferable and allow rapid mapping of SAV
451 communities on larger scales in similar river environments. There is significant room to improve the
452 classification results, as the overall accuracy values were not high. However, we think the
453 performance of the classification rule set should be seen in the light of the specific complications of
454 the submerged aquatic environment for which the classification was performed, complex mixtures of
455 vegetation species present in the three images, as well as the image data quality issues discussed
456 above. We therefore recommend that the approach is investigated more widely in order to further
457 explore its potential.

458 Although the authors tried to avoid using absolute spectral values, which are directly dependent on
459 changes in illumination conditions in an image, it appeared not possible to fully achieve this. With
460 changes in illumination conditions or similarly changes in water transparency thresholds based on
461 these values, will need to be adjusted. By including such thresholds as variables within the rule set,
462 they can easily be adjusted by adaptation of the master rule set and so avoiding having to develop rule
463 sets from scratch (Tiede et al., 2010b). In similar ways adaptations to the rule set can be made to

464 compensate for changes in scale with changes in elevation of the camera used, which will affect
465 features based on (absolute) size and shape values. Also a more automated/objective object scale
466 parameter optimization, similar to the method used by Anders et al. (2011) may make the OBIA
467 approach more robust.

468 When the rule set proves sufficiently robust over space and time the process can easily be scaled up
469 and is only limited by the ability of a researcher to collect photographs of sufficient resolution. With
470 currently available quality of digital cameras, photos will still have to be collected from relatively low
471 altitude, which results in relatively small image footprints (app. 5 x 5 m). Only suitable platforms for
472 data collection are therefore telescopic masts/poles or rotary winged UAS-s that can operate
473 sufficiently close to the water surface. Rapid sensor development is likely to remove this limitation in
474 the near future. Considering the relatively low dimensionality of the image data (app. < 6 image
475 bands) data volume is thought not to be a problem.

476 The rule-based classification using expert knowledge is relatively intuitive and can be made
477 accessible to and can be amended by people without remote sensing expertise. It is even highly
478 recommendable to discuss image classifications with aquatic plant experts as their knowledge and
479 cognitive processes to recognize submerged plant species can be used in the classification rule
480 development process. Using the software to write the rule sets and execute the classification does
481 however involve a steeper learning curve and will still require assistance of a remote sensing
482 specialist.

483 Progress in knowledge based classification

484 As mentioned by Tiede et al. (2010a:194) modelling target classes doesn't just require computational
485 skill, but also a wealth of knowledge 'about the area and the composition of the image setting'.

486 However, as summarized by Arvor et al. (2013), the OBIA knowledge-based approach suffers from
487 various weaknesses, including the 'blackbox' approach of the image segmentation part of the OBIA
488 workflow, but in particular the subjectivity of knowledge and understanding, since all experts have
489 their own conceptualization of the reality they try to map from an image. To resolve the latter issue,

490 the remote sensing community should therefore endeavour to go beyond this approach and start
491 working with more universal ontologies in combination with tools such as automatic target
492 recognition (ATR) algorithms. Such approaches should be evaluated on their ability to reproduce the
493 reasoning of experts (Arvor et al., 2013).

494 Evaluation of many remote sensing based classifications are currently hampered by the availability of
495 reference data. On screen manually delineated classifications/maps are often used for this purpose as
496 they are seen as the most reliable information available. Particularly for SAV, classifications derived
497 manually from remote sensing data are currently the only reliable option available (Husson et al.,
498 2014). However there is reason to question this reliance on manually mapped class boundaries, as
499 they will not be error free, in particular when species form a mixed surface cover as in the current
500 study. There will be a limit to what extent the expert can separate between species, influenced by the
501 time they spend working on the task and their personal concept of reality. We would like to argue that
502 by creating boundaries through a clear set of rules, as is done in OBIA, a more objective interpretation
503 of an image is possible.

504 Conclusion

505 This paper described a first attempt at species level classification of SAV, using VHR image data and
506 multi-level knowledge-based OBIA analysis. It demonstrated how VHR image data and the OBIA
507 approach can be used to obtain consistent classifications of submerged aquatic vegetation in shallow
508 clear-water streams, using a single object-based classification rule set. The best classification result of
509 61% overall accuracy was slightly less than what has been achieved with more conventional methods,
510 such as manual mapping (Husson et al., 2014) or the nearest neighbour algorithm (e.g. Roelfsema et
511 al., 2014). However, it needs to be seen in the light of the complex study environment that was
512 tackled, as well as the benefit of transferability of the approach.

513 Furthermore the use of relatively low-tech remote sensing equipment, the sub-optimal weather
514 conditions during data collection, as well as the heterogeneous vegetation composition of the studied

515 sites, made data collection and analysis particularly challenging. We therefore think that our results
516 showed that OBIA has great potential to aid detailed classification of highly biodiverse streams at
517 species level. We even expect that the method can provide an objective quantitative assessment of
518 mixed vegetation cover that may be difficult to map/monitor in other ways. However, to confirm this
519 a more detailed comparison needs to be made of the classification accuracy of the OBIA analysis,
520 while providing an assessment of the reliability of the reference data. This presents an interesting
521 challenge in itself.

522 Acknowledgments

523 Funding for this project was provided by the FWO (Fund for Scientific Research) – Flanders
524 (Belgium) – (G.0290.10) via the multidisciplinary research project ‘Linking optical imaging
525 techniques and 2D-modelling for studying spatial heterogeneity in vegetated streams and rivers’
526 (Antwerp University, Ghent University, 2010-2013), the FWO Scientific Research Community
527 ‘Functioning of river ecosystems by plant-flow-sediment interactions’. V.V. thanks the Institute for
528 the Promotion of Innovation through Science and Technology in Flanders (IWT-Vlaanderen) for
529 personal research funding. J.S. is a postdoctoral fellow of FWO (project no. 12H8616N).

530 References

- 531 Anders, N. S., A. C. Seijmonsbergen & W. Bouten, 2011. Segmentation optimization and stratified
532 object-based analysis for semi-automated geomorphological mapping. *Remote Sensing of*
533 *Environment* 115: 2976–2985.
- 534 Anderson, K. & K. J. Gaston, 2013. Lightweight unmanned aerial vehicles will revolutionize spatial
535 ecology. *Frontiers in Ecology and the Environment* 11: 138–146.
- 536 Arvor, D., L. Durieux, S. Andrés & M-A. Laporte, 2013. Advances in Geographic Object-Based
537 Image Analysis with ontologies: A review of main contributions and limitations from a remote
538 sensing perspective. *ISPRS Journal of Photogrammetry and Remote Sensing* 82: 125–137.

539 Belgiu, M., I. Tomljenovic, T. Lampoltshammer, T. Blaschke & B. Höfle, 2014. Ontology-Based
540 Classification of Building Types Detected from Airborne Laser Scanning Data. *Remote Sensing* 6:
541 1347–1366.

542 Blaschke, T., 2010. Object based image analysis for remote sensing. *ISPRS Journal of*
543 *Photogrammetry and Remote Sensing* 65: 2–16.

544 Blaschke, T., K. Johansen & D. Tiede, 2011. Object based image analysis for vegetation mapping and
545 monitoring. In Qihao Weng (ed), *Advances in environmental remote sensing: Sensors, algorithms,*
546 *and applications*. CRC Press, Taylor and Francis, United States: 141–266.

547 Blaschke, T., G. J. Hay, M. Kelly, S. Lang, P. Hofmann, E. Addink, R. Queiroz Feitosa, F. van der
548 Meer, H. van der Werff, F. van Coillie & D. Tiede, 2014. Geographic Object-Based Image Analysis –
549 Towards a new paradigm. *ISPRS Journal of Photogrammetry and Remote Sensing* 87: 180–191.

550 Definiens AG, 2007. *Definiens Developer 7 - Reference Book*.
551 <http://www.ecognition.cc/download/ReferenceBook.pdf>

552 d’Oleire-Oltmanns, S., I. Marzloff, D. Tiede & T. Blaschke, 2014. Detection of Gully-Affected Areas
553 by Applying Object-Based Image Analysis (OBIA) in the Region of Taroudannt, Morocco. *Remote*
554 *Sensing* 6: 8287–8309.

555 Drăguț, L., D. Tiede, & S. R. Levick, 2010. ESP: a tool to estimate scale parameter for
556 multiresolution image segmentation of remotely sensed data. *International Journal of Geographical*
557 *Information Science* 24: 859–871.

558 Dronova, I., 2015. Object-Based Image Analysis in Wetland Research: A Review. *Remote Sensing* 7:
559 6380–6413.

560 Dronova, I., P. Gong, N. E. Clinton, L. Wang, W. Fu, S. Qi & Y. Liu, 2012. Landscape analysis of
561 wetland plant functional types: The effects of image segmentation scale, vegetation classes and
562 classification methods. *Remote Sensing of Environment* 127: 357–369.

563 Foody, G. M., 2002. Status of land cover classification accuracy assessment. *Remote Sensing of*

564 Environment 80: 185– 201.

565 Hauet, A., M. Muste & H-C. Ho, 2009. Digital mapping of riverine waterway hydrodynamic and
566 geomorphic features. *Earth Surface Processes and Landforms* 34: 242-252.

567 Husson, E., O. Hagner & F. Ecke, 2014. Unmanned aircraft systems help to map aquatic vegetation.
568 *Applied Vegetation Science* 17: 567–577.

569 Kay, S., J. D. Hedley & S. Lavender, 2009. Sun Glint Correction of High and Low Spatial Resolution
570 Images of Aquatic Scenes: a Review of Methods for Visible and Near-Infrared Wavelengths. *Remote*
571 *Sensing* 1: 697–730.

572 Klemas, V., 2013. Remote Sensing of Coastal Wetland Biomass: An Overview. *Journal of Coastal*
573 *Research* 290: 1016–1028.

574 Laliberte, A. S., M. A. Goforth, C. M. Steele & A. Rango, 2011. Multispectral Remote Sensing from
575 Unmanned Aircraft: Image Processing Workflows and Applications for Rangeland Environments.
576 *Remote Sensing* 3: 2529–2551.

577 Laliberte, A. S., A. Rango, J. E. Herrick & E. L. Fredrickson, 2007. An object-based image analysis
578 approach for determining fractional cover of senescent and green vegetation with digital plot
579 photography. *Journal of Arid Environments* 69: 1–14.

580 Li, X. & G. Shao, 2014. Object-Based Land-Cover Mapping with High Resolution Aerial
581 Photography at a County Scale in Midwestern USA. *Remote Sensing* 6: 11372–11390.

582 Lucas, M. & J. Goodman, 2014. Linking Coral Reef Remote Sensing and Field Ecology: It’s a Matter
583 of Scale. *Journal of Marine Science and Engineering* 3: 1–20.

584 Lucieer, A., Z. Malenovsky, T. Veness & L. Wallace, 2014. HyperUAS-Imaging Spectroscopy from a
585 Multirotor Unmanned Aircraft System. *Journal of Field Robotics* 31: 571–590.

586 Luscier, J. D., W. L. Thompson, J. M. Wilson, B. E. Gorham & L. D. Drăguț, 2006. Using digital
587 photographs and object-based image analysis to estimate percent ground cover in vegetation plots.
588 *Frontiers in Ecology and the Environment* 4: 408–413.

589 Mui, A., Y. He & Q. Weng, 2015. An object-based approach to delineate wetlands across landscapes
590 of varied disturbance with high spatial resolution satellite imagery. *ISPRS Journal of Photogrammetry
591 and Remote Sensing* 109: 30–46.

592 Olofsson, P., G. M. Foody, M. Herold, S. V. Stehman, C. E. Woodcock, & M. A. Wulder, 2014. Good
593 practices for estimating area and assessing accuracy of land change. *Remote Sensing of Environment*
594 148: 42–57.

595 Radoux, J., P. Bogaert, D. Fasbender, & P. Defourny, 2011. Thematic accuracy assessment of
596 geographic object-based image classification. *International Journal of Geographical Information
597 Science* 25: 895-911.

598 Rampi, L. P., J. F. Knight & K. C. Pelletier, 2014. Wetland Mapping in the Upper Midwest United
599 States. *Photogrammetric Engineering & Remote Sensing* 80: 439–448.

600 Roelfsema, C. M., M. Lyons, E. M. Kovacs, P. Maxwell, M. I. Saunders, J. Samper-Villarreal & S. R.
601 Phinn, 2014. Multi-temporal mapping of seagrass cover, species and biomass: A semi-automated
602 object based image analysis approach. *Remote Sensing of Environment* 150: 172–187.

603 Tiede, D., S. Lang, F. Albrecht & D. Hölbling, 2010a. Object-based Class Modeling for Cadastre-
604 constrained Delineation of Geo-objects. *Photogrammetric Engineering & Remote Sensing* 76: 193–
605 202.

606 Tiede, D., S. Lang, D. Hölbling & P. Füreder, 2010b. Transferability of OBIA rule sets for IDP camp
607 analysis in Darfur. *The International Archives of the Photogrammetry, Remote Sensing and Spatial
608 Information Sciences*, XXXVIII-4/C7.

609 Verhoeven, G., 2008. Imaging the invisible using modified digital still cameras for straightforward
610 and low-cost archaeological near-infrared photography. *Journal of Archaeological Science* 35: 3087–
611 3100.

612 Verhoeven, G. J. J., 2010. It's all about the format – unleashing the power of RAW aerial
613 photography. *International Journal of Remote Sensing* 31: 2009–2042.

614 Visser, F., K. Buis, V. Verschoren & P. Meire, 2015. Depth Estimation of Submerged Aquatic
615 Vegetation in clear water streams using low-altitude optical remote sensing. *Sensors* 15: 25287–
616 25312.

617 Visser, F., C. Wallis & A. M. Sinnott, 2013. Optical remote sensing of submerged aquatic vegetation:
618 Opportunities for shallow clearwater streams. *Limnologica - Ecology and Management of Inland*
619 *Waters* 43: 388–398.

620 Woodget, A. S., P. C. Carbonneau, F. Visser & I. Maddock, 2015. Quantifying submerged fluvial
621 topography using hyperspatial resolution UAS imagery and structure from motion photogrammetry.
622 *Earth Surface Processes and Landforms* 40: 47–64.

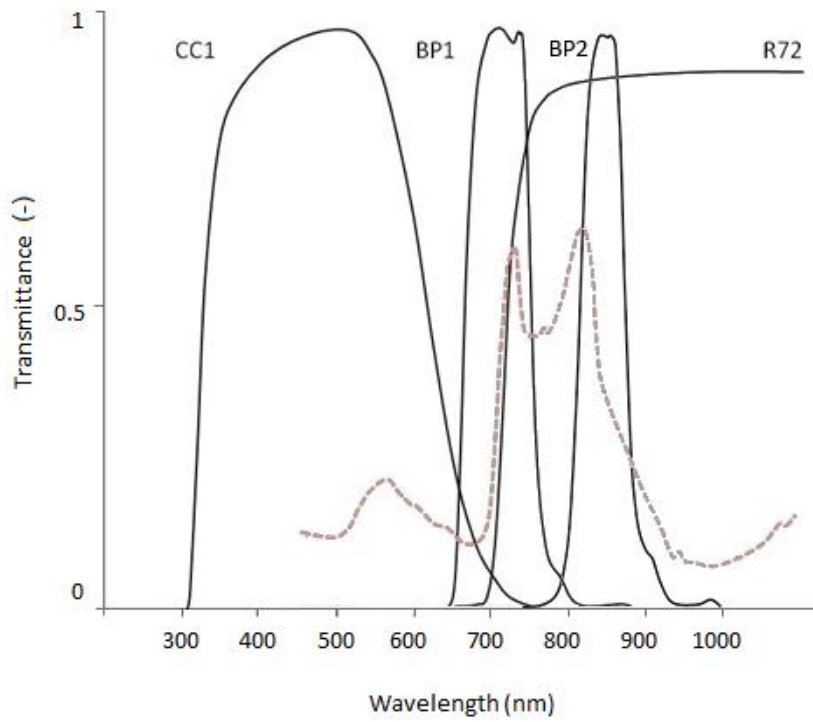
623 **Figures**



624

625 **Fig. 1** Colour photo of *C. obtusangula* (l) and *R. aquatilis* (r) patches. River flow direction is left to
626 right. Despite the relatively similar leaf colour the plants can be distinguished due to variation in plant
627 morphology

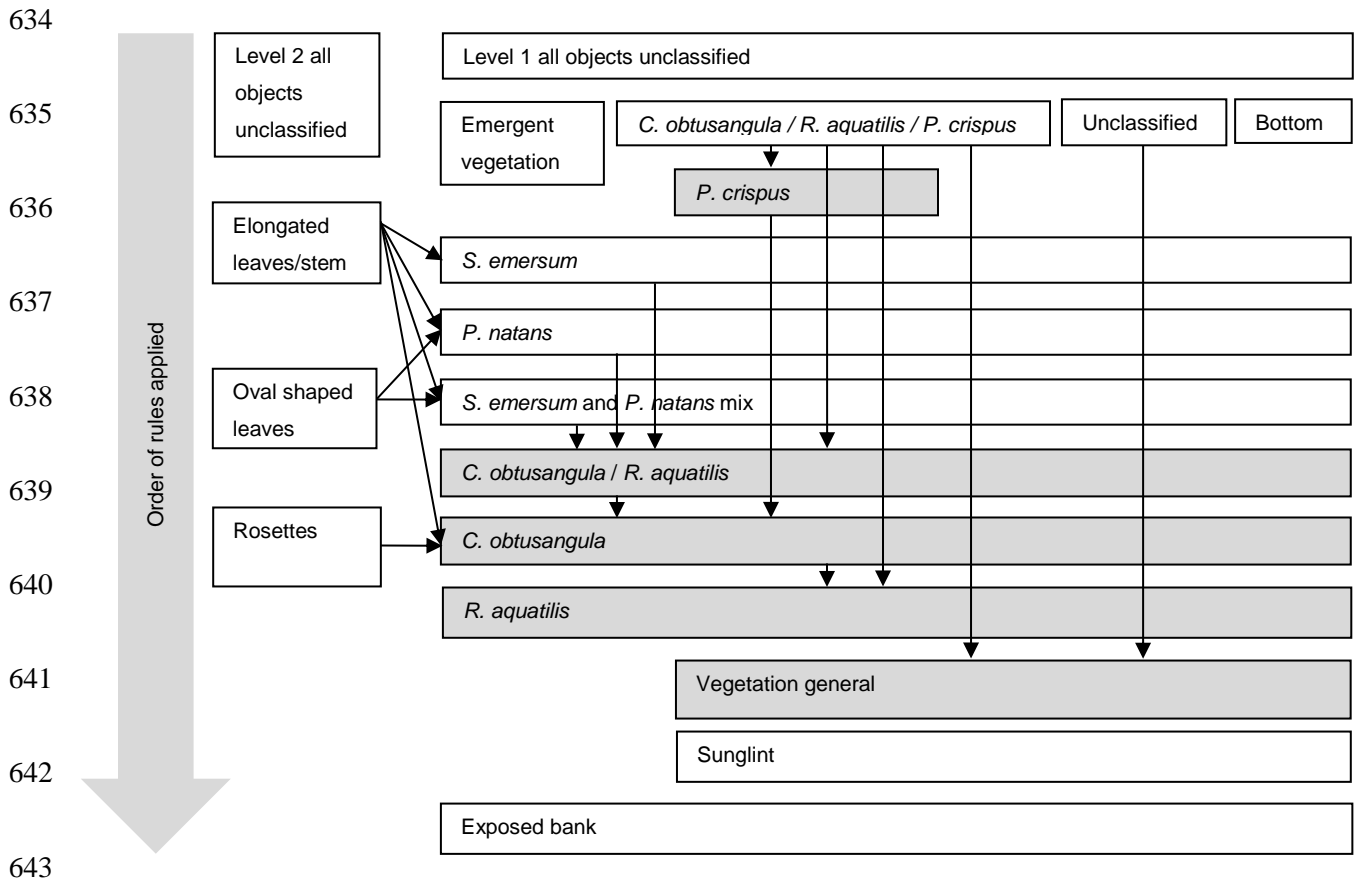
628



629

630 **Fig. 2** Transmission spectra of NIR(BP1) and NIR(BP2) bandpass filters and CC1 and NIR(R72)
 631 blocking filters based on manufacturers specifications (LDP LLC, Carlstadt, USA). Submerged
 632 macrophyte spectrum included with dashed line for comparison (source: Visser et al., 2015)

633



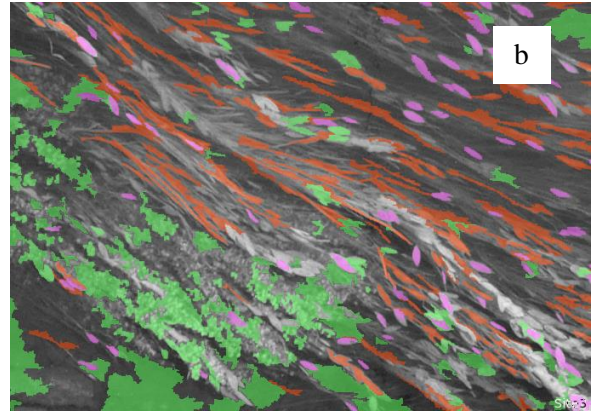
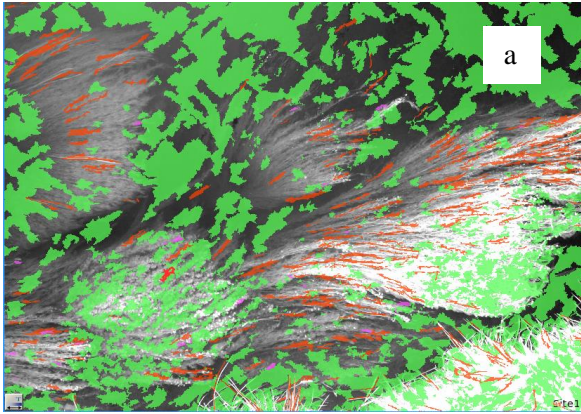
644 **Fig. 3** Flow diagram illustrating the structure of the rule set used to classify objects into the

645 designated classes. Classes shown in grey are created using objects from only a limited range of

646 existing classes as input. These source classes are indicated with arrows. Classes shown in white were

647 created using all objects in the classification process.

648



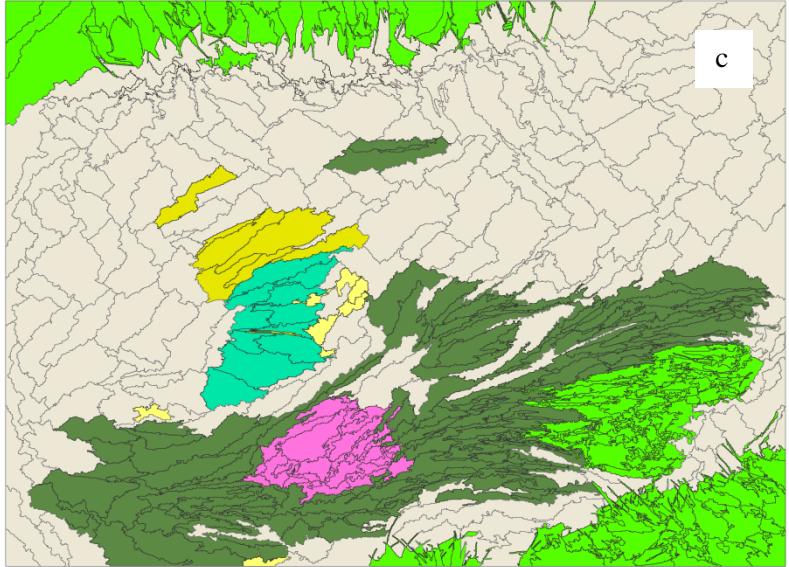
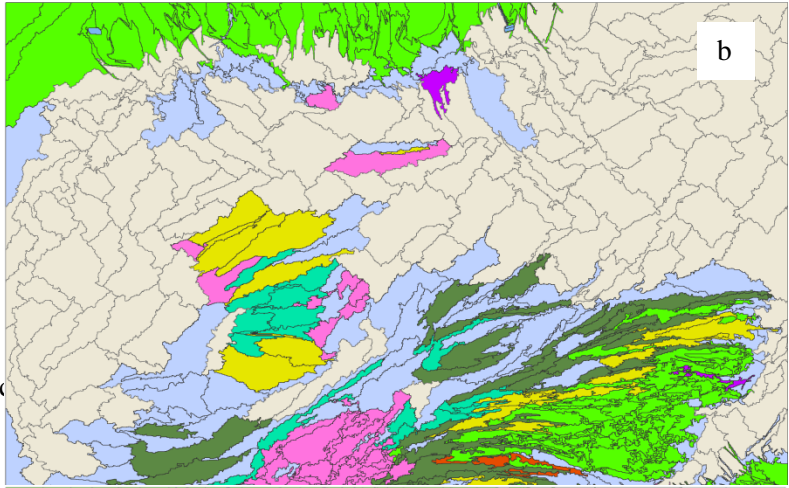
649

-  Oval shaped leaves
-  Rosettes
-  Elongated leaves/stems

650

651 **Fig. 4** Level 2 classification of site 1 showing Rosette objects (a and b), Elongated leaf/stem objects (a
652 and b) and Oval shaped leaves (b)

653
654
655
656
657
658
659
660
661
662
663
664
665
666
667
668
669
670

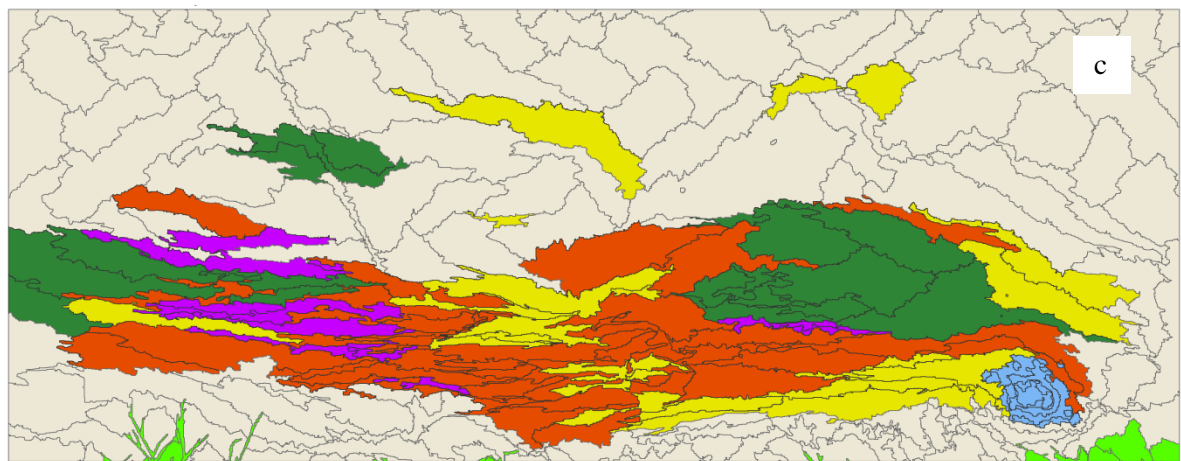
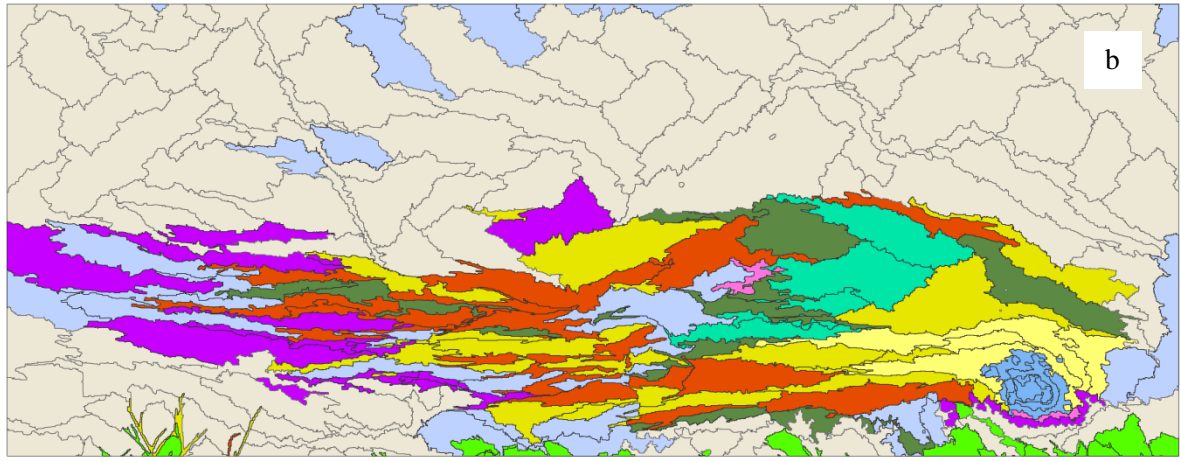


- Bank/emergent vegetation
- Bar
- Bottom
- C. obtusangula*
- Sunlint
- S. emersum* and *P. natans* mix
- Exposed bank/Oat flakes
- P. crispus*
- P. natans*
- R. aquatilis*
- S. emersum*
- Vegetation general

671 **Fig. 5** Site 1 NIR(BP1) image (a), OBIA classification (b) and manual classification (c)

672

673
 674
 675
 676
 677
 678
 679
 680
 681
 682
 683
 684
 685
 686
 687
 688
 689
 690
 691
 692



0 1 m



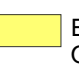




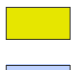




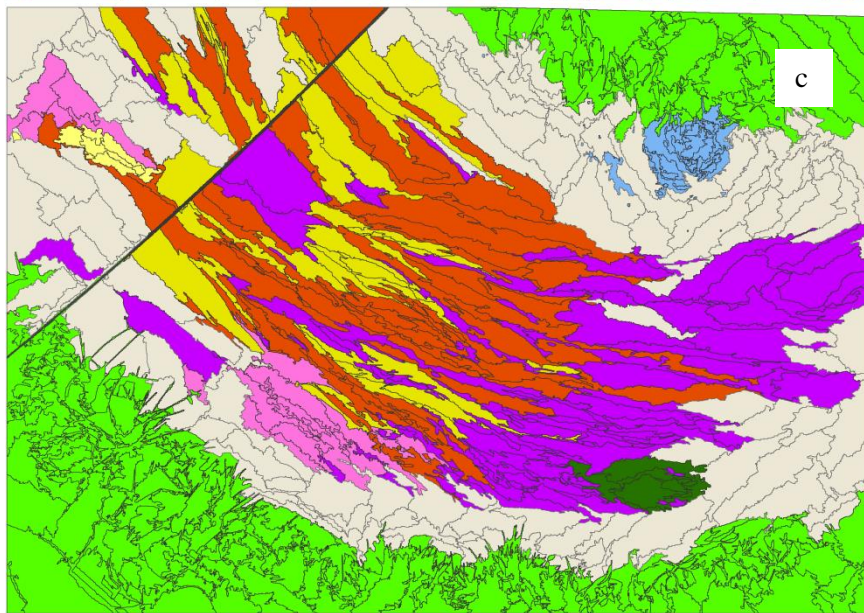
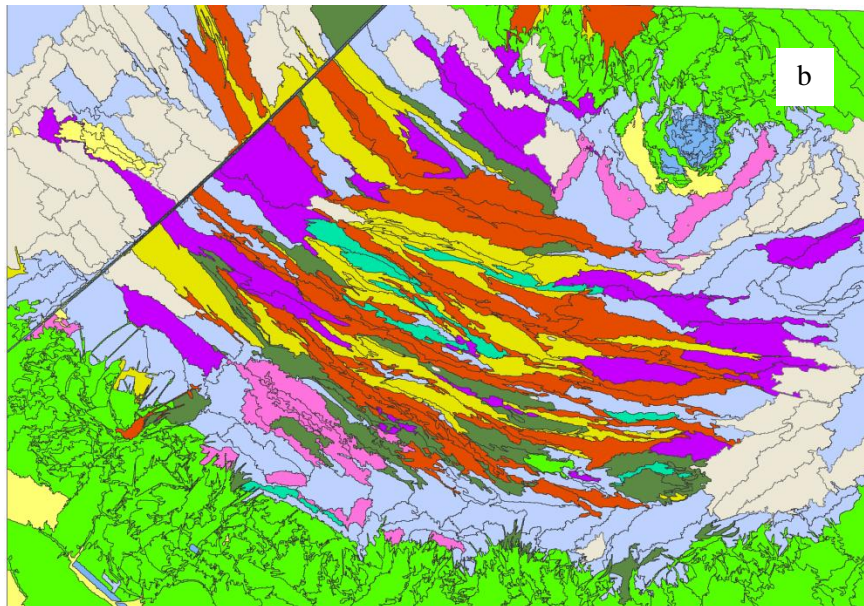
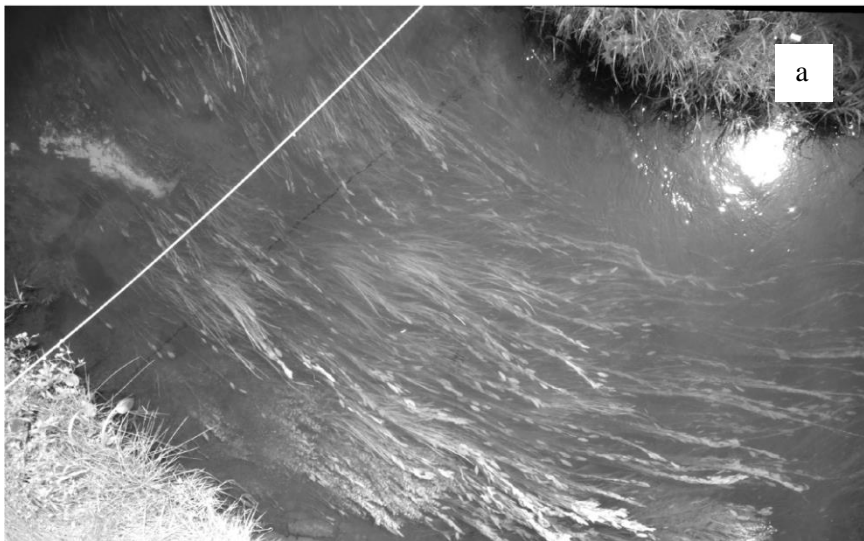
- | | | | |
|--|--|--|--|
|  Bank/emergent vegetation |  <i>C. obtusangula</i> |  Exposed bank/ Oat flakes |  <i>R. aquatilis</i> |
|  Bar |  Sunlint |  <i>P. crispus</i> |  <i>S. emersum</i> |
|  Bottom |  <i>S. emersum</i> and <i>P. natans</i> mix |  <i>P. natans</i> |  Vegetation general |

Fig. 6 Site 2 NIR(BP1) image (a), OBIA classification (b) and manual classification (c)

693
694
695
696
697
698
699
700
701
702
703
704
705
706
707
708
709
710
711















-  Bank/emergent vegetation
-  Bar
-  Bottom
-  *C. ostusangula*
-  Sun glint
-  *S. emersum* and *P. natans* mix
-  Exposed bank/Oat flakes
-  *P. crispus*
-  *P. natans*
-  *R. aquatilis*
-  *S. emersum*
-  Vegetation general

Fig. 7 Site 3 NIR(BP1) image (a), OBIA classification (b) and manual classification (c)

713 **Tables**

714 **Table 1** Rules and thresholds used to assign objects for all classes used. Classes including (f) are final
 715 classes as used on the final maps. Classes including (t) are intermediate classes used in the
 716 classification process. All classes were created at segmentation level 1, unless ‘L2’ is included
 717 indicating the class was created at Level 2. Rules marked with (*) rely on absolute reflectance values

Class name	Rules + thresholds applied
Bank/emergent vegetation (f)	*Mean NIR(R72) > 160 NDVI >= 0
Bottom (f)	*Mean NIR(BP2) < 35 Standard deviation NIR(R72) < 4.5
<i>C. obtusangula/R. aquatilis/P. crispus</i> (t)	*Mean NIR(BP1) > 65
<i>C. obtusangula / R. aquatilis</i> (t)	Mean curvature/Length sub objects > 5.5 Mean L/W ratio sub objects < 4 *135 < Mean red < 155
Rosettes (L2, t)	Length/width ratio < 2
Elongated leaves/stems (L2, t)	Length/width > 1 *Mean NIR(BP1) > 60 Relative border to brighter objects NIR(BP1) < 0.5 Width < 18 pxl
Oval shaped leaves (L2, t)	Area < 450 pxl 90 < Brightness < 134 Eliptic fit > 0.65 Length < 50 pxl 1.5 < Length/Width < 4 Mean difference to neighbours NIR(BP1) > 6 Roundness < 1.2
<i>C. obtusangula</i> (f)	Number of elongated leaves/stems < 2 Relative area of rosettes > 0.23
<i>S. emersum</i> (f)	Mean curvature/Length sub objects < 5.4 Number of oval shaped leaves <= 1 Or Number of elongated leaves/stems > 2 Relative area elongated leaves/stems > 0.4

<i>P. natans</i> (f)	Number of oval shaped leaves > 1 Relative area elongated leaves/stems <= 0.4
<i>P. natans</i> and <i>S. emersum</i> mix (f)	Number of oval shaped leaves > 1 Relative area of elongated leaves/stems > 0.4 Or Number of elongated leaves/stems > 2 Relative area elongated leaves/stems > 0.4
<i>R. aquatilis</i> (f)	Number of elongated leaves/stems > 1
<i>P. crispus</i> (f)	*3 < Standard deviation NIR(BP1) < 5.5
Vegetation general (f)	*Standard deviation NIR(BP2) > 3
Exposed bank (f)	*Mean Red > 190
Sunglint (f)	Brightness > 160 NDVI < 0

718

719 **Table 2** Accuracy values for the OBIA classifications compared to a manually delineated
720 classification

Overall Accuracy (%)	
Site 1	(304/496)*100 =61
Site 2	(149/241)*100 = 61
Site 3	(309/580)*100 = 53

721

722

723

724

725

726

727

728 **Table 3** Error matrices showing for each class the number of correctly classified polygons and the
 729 alternative class allocation of misclassified polygons, for sites 1 (a), 2 (b) and 3 (c)

a) Site 1														
<i>Manual delineation:</i>														
	Bank/emergent	Bottom	<i>C. obtusangula</i>	<i>P. crispus</i>	<i>S. emersum</i>	Sunglint	<i>S. emersum</i> and <i>P. natans</i> mix	<i>P. natans</i>	Exposed bank	<i>R. aquatilis</i>	Vegetation general	Total	User's accuracy	Errors of commission
Classification:														
Bank/emergent	107	1	4	0	2	7	0	1	1	4	14	141	0.76	0.24
Bottom	5	140	2	0	1	0	1	2	0	3	50	204	0.69	0.31
<i>C. obtusangula</i>	1	0	13	0	0	0	0	0	0	0	3	17	0.76	0.24
<i>P. crispus</i>	0	0	0	7	3	0	0	0	0	0	1	11	0.64	0.36
<i>S. emersum</i>	0	1	1	1	4	0	0	0	0	0	1	8	0.50	0.50
Sunglint	0	0	0	0	0	0	0	0	0	0	0	0	-	-
<i>S. emersum</i> and <i>P. natans</i> mix	0	0	0	0	0	0	0	0	0	0	0	0	-	-
<i>P. natans</i>	0	0	0	0	0	0	0	0	0	0	0	0	-	-
Exposed bank	0	0	3	0	0	0	0	0	1	0	1	5	0.20	0.80
<i>R. aquatilis</i>	14	1	3	6	9	0	2	4	0	32	39	110	0.29	0.71
Vegetation general	0	0	0	0	0	0	0	0	0	0	0	0	-	-
Total	127	143	26	14	19	7	3	7	2	39	109	496		
Producer's accuracy	0.84	0.98	0.50	0.50	0.21	0.00	0.00	0.00	0.50	0.82	0.00			
Errors of omission	0.16	0.02	0.50	0.50	0.79	1.00	1.00	1.00	0.50	0.18	1.00			

730
 731
 732
 733
 734
 735
 736
 737

b) Site 2		Manual delineation:												
	Bank/emergent	Bottom	<i>C. obtusangula</i>	<i>P. crispus</i>	<i>S. emersum</i>	Sunglint	<i>S. emersum</i> and <i>P. natans</i> mix	<i>P. natans</i>	Exposed bank	<i>R. aquatilis</i>	Vegetation general	Total	User's accuracy	Errors of commission
Classification:														
Bank/emergent	16	0	0	0	2	0	2	0	0	0	0	20	0.8	0.2
Bottom	7	96	0	0	0	0	0	3	1	2	17	126	0.76	0.24
<i>C. obtusangula</i>	0	0	0	0	0	0	0	0	0	0	0	0	-	-
<i>P. crispus</i>	0	0	0	0	0	0	0	0	0	0	0	0	-	-
<i>S. emersum</i>	0	4	0	0	9	0	4	0	1	2	2	22	0.41	0.59
Sunglint	0	0	1	0	0	8	0	0	1	0	0	10	0.8	0.2
<i>S. emersum</i> and <i>P. natans</i> mix	0	2	0	1	7	0	8	2	2	3	7	32	0.25	0.75
<i>P. natans</i>	0	0	0	1	1	0	1	7	0	1	1	12	0.58	0.42
Exposed bank	0	0	0	0	0	0	0	0	0	0	0	0	-	-
<i>R. aquatilis</i>	0	2	1	3	1	0	1	1	0	5	5	19	0.26	0.74
Vegetation general	0	0	0	0	0	0	0	0	0	0	0	0	-	-
Total	23	104	2	5	20	8	16	13	5	13	32	241		
Producer's accuracy	0.70	0.92	0	0	0.45	1	0.5	0.54	0	0.38	0			
Errors of omission	0.30	0.08	1	1	0.55	0	0.5	0.46	1	0.62	1			

738

739

740

741

742

743

744

745

746

747

748

749

750

c) Site 3

Manual delineation:

	Bank/emergent	Bottom	<i>C. obtusangula</i>	<i>P. crispus</i>	<i>S. emersum</i>	Sunglint	<i>S. emersum</i> and <i>P. natans</i> mix	<i>P. natans</i>	Exposed bank	<i>R. aquatilis</i>	Vegetation general	Bar	Total	User's accuracy	Errors of commission
Classification:															
Bank/emergent	182	1	2	0	4	4	3	0	5	7	16	0	224	0.81	0.19
Bottom	2	35	7	1	0	0	0	4	2	1	67	0	119	0.29	0.71
<i>C. obtusangula</i>	0	2	8	0	0	0	0	0	0	4	3	0	17	0.47	0.53
<i>P. crispus</i>	0	0	0	0	0	0	0	0	0	0	0	0	0	-	-
<i>S. emersum</i>	0	6	0	2	17	0	1	0	0	4	6	0	36	0.47	0.53
Sunglint	11	11	0	0	0	11	0	1	4	0	1	0	39	0.28	0.72
<i>S. emersum</i> and <i>P. natans</i> mix	0	3	0	3	9	0	23	3	0	5	4	0	50	0.46	0.54
<i>P. natans</i>	1	3	1	2	10	0	15	17	0	12	24	0	85	0.20	0.80
Exposed bank	0	0	0	0	0	0	0	0	4	0	0	0	4	1.00	0.00
<i>R. aquatilis</i>	0	0	0	1	0	0	0	0	0	4	1	0	6	0.67	0.33
Vegetation general		0	0	0	0	0	0	0	0	0	0	0	0	-	-
Bar	0	0	0	0	0	0	0	0	0	0	0	8	8	1.00	0.00
Total	196	61	18	9	40	15	42	25	15	37	122	1.00	580		
Producer's accuracy	0.93	0.57	0.44	0.00	0.43	0.73	0.55	0.68	0.27	0.11	0.00	0.00			
Errors of omission	0.07	0.43	0.56	1.00	0.58	0.27	0.45	0.32	0.73	0.89	1.00	0.00			

751